Journal of Engineering Mechanics and Machinery (2024)
Clausius Scientific Press, Canada

DOI: 10.23977/jemm.2024.090214
ISSN 2371-9133 Vol. 9 Num. 2

Numerical investigation on the aerodynamic characteristics of the multi-blade propellers under different inflow conditions

Xinming Huang

School of Mechanical Engineering, Hunan University of Science and Technology, Xiangtan, 411201, China

Keywords: Airflow simulation, Different-propeller blade type, Multi-propellers, Inflow conditions, Aerodynamic characteristics

Abstract: EVTOL (Electric Vertical Take-off and Landing) vehicles have the advantages of no runway for take-off, high safety, low noise, zero-emission, easy maintenance, and low cost after scale operation. Under the background of the global development of a low-altitude economy, the demand for eVTOL is expected to grow rapidly. Propellers with different blade numbers are modelled, and the aerodynamic characteristics of three, four, five, and six-bladed propellers under uniform airflow environment conditions are analysed. The pressure values on the surface of each propeller blade were determined by simulating the airflow environment. The performance characteristics of the four propellers under different airflow conditions were numerically investigated. A prototype blade model was fabricated in an aerodynamic wind tunnel, and experimental values of aerodynamic pressures were obtained through calculations and simulations. The computational results help to provide insight into the physical characteristics of the airflow around the propeller blade and the resulting performance metrics.

1. Introduction

In recent years, as the population of the world's major cities continues to increase, urban ground transportation road construction has gradually saturated, and the existing urban transportation model faces the limitations of urban transportation and increasingly severe travel congestion. Compared with jet propulsion devices, propeller propulsion devices with high propulsion efficiency and low fuel consumption have received more and more attention and have ushered in new development opportunities [1][2]. Low-altitude vehicles need to use propellers as the main propulsion method or the main control means in order to achieve long-lasting and smooth flight[3]. The dynamic characteristics of the propeller system, which is the power system of a rotorcraft, are essential factors that must be carefully considered in design and control[4]. Although propellers need to be efficient in terms of vehicle range and take-off weight, they can overcome challenges such as energy storage density and geometrical constraints, so designing an optimized propeller blade structure is an effective way to improve efficiency[5].

Typically, simulation software performs preliminary data investigations by constructing models

of actual environments and is commonly used for various topics. Regardless of the research area, geometric models can be designed and analyzed by computer-aided design[6]. Most of the existing studies test and analyze the aerodynamic factors of the same paddle model at different sizes and levels and rarely address the aerodynamic performance gap of the same paddle model at different numbers of paddles. For example, Liu et al. took the aeronautical propellers as an entry point to explore the aerodynamic and aerodynamic noise problems during their operation, starting from improving propeller propulsion efficiency and solving the noise pollution problem[7]. Nilavarasan et al. analyzed the angle of attack of flaps located at the trailing edge of the propeller at 45 and 90 degrees to the chord line of the propeller, respectively, and the results of the study concluded that a significant increase in the coefficient of lift, and a reduction in the angle of attack could improve the aerodynamic efficiency of the propeller[8]. To study the effect of propeller arrangement position on the aerodynamic characteristics of the aircraft, Ivan Kostić determined the optimal blade positions for several asymmetric airfoils by algorithmic analysis and analyzed their effects on the aerodynamic characteristics of the aircraft [9].

This paper investigates a propeller model with different numbers of blades through finite element analysis. The specific values of the pressure load are generated by the airflow around the surface of the above-constructed propeller structure, which are analyzed and compared to the aerodynamic performances of the propellers with different geometrical shapes.

2. Structural design of multi-propellers

Based on the previous literature[10], the relationship between the propulsion efficiency of a typical propeller and its number of blades is shown in Figure 1. It can be seen that the cruise propulsion efficiency of the two-blade and three-blade is approximately equal, but the climbing propulsion efficiency of the three-blade propeller is much higher. The two-blade propellers are primarily used in multi-rotor structures, while only a few large-tonnage vehicles in the field of eVTOL use multi-rotor propellers, and the operational stability of the two-blade propellers is not as good as that of the three-blade propellers.

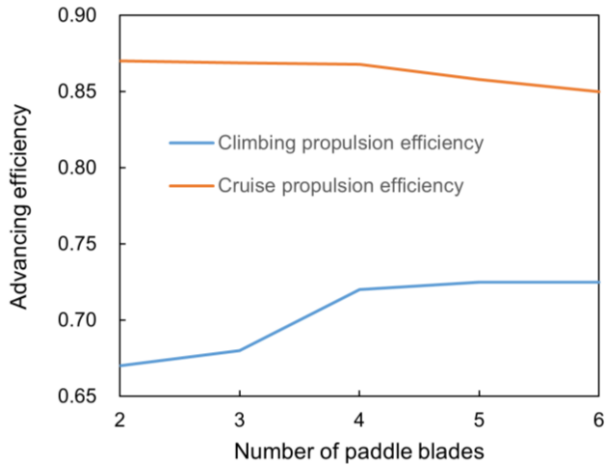

Figure 1: Variations of propeller propulsion efficiency with blade numbers[10]

In eVTOLs, a few large-tonnage vehicles use multi-rotor propellers, and the operational stability of two-blade propellers is not as good as that of three-blade propellers. Therefore, this paper focuses on the aerodynamic performance of three-bladed, four-bladed, five-bladed and six-bladed propellers. The optimum number of blades for the propeller is 4 in combination with the climb propulsion efficiency and the cruise propulsion efficiency. Table 1 summarises the detailed geometrical parameters of the four established propellers.

Table 1: Geometric parameters of multi-blade propeller used in this study

Designation	**Type**	**Diameter (D_p)/m**	**Chord length ($c_{0.7Rp}$)/m**	**Paddle angle (°)**
Value	Fixed pitch	1.0400 m	0.2405 m	41.16
Designation	**Pitch ratio(P/D_p)($0.7R_p$)**	**Number of blades**	**Rotation(seen from downstream)**	**Oar head angle /(°)**
Value	0.36	3, 4, 5, 6	Clockwise	22.81

The finite element modelling adopts the control univariate method, which takes the number of propeller blades as the only variable, so all four models are manufactured with the same material. Composite propeller blades have outstanding advantages in weight reduction and noise reduction compared with metal propeller blades. Compared to duralumin propellers, composites can reduce weight by about 50%[11]. The total and directional deformations of carbon and glass fibers are proportional to the load, but the deformations and stresses of propellers made of carbon fibers are greater than those of glass fibers[12]. Four propeller models with different blades are established by using Solidworks software and E glass fiber material, and the specific model structure is shown in Figure. 2.

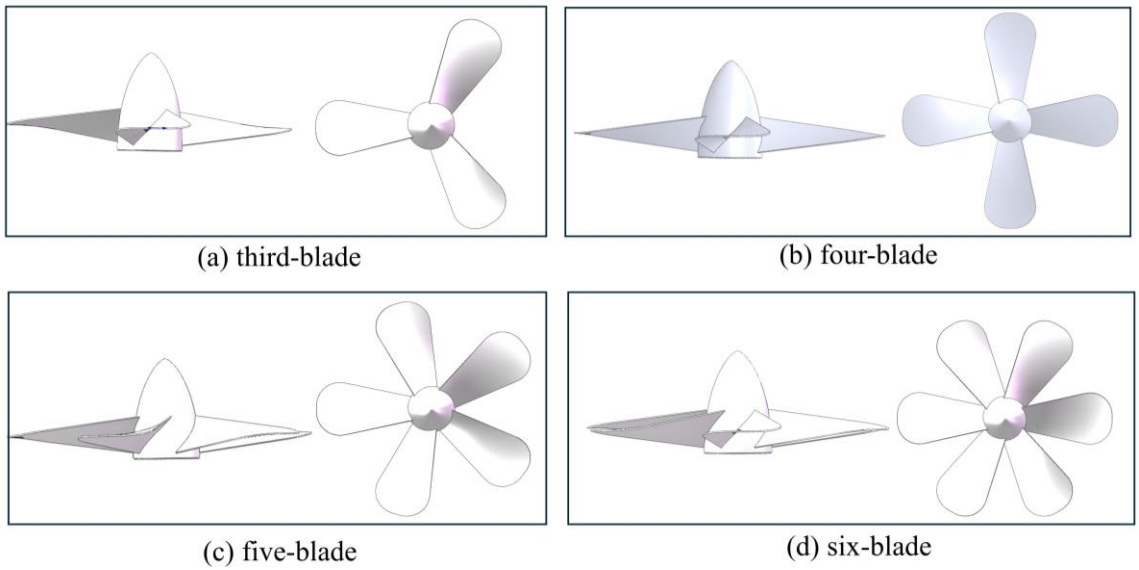

Figure 2: Geometric modelling of propellers with four structures: (a) third blade, (b) four-blade, (c) five-blade, (d) six-blade

3. Finite element modelling

Four kinds of geometrical structure blades are established in Solidworks: three-blade, four-blade, five-blade and six-blade, as shown in Figure 3. Four models are made of E-glass fiber material, and the x.t suffix file is output and imported into Workbench software to define the physical field boundary conditions of the inlet, outlet, fluid, and rota, of which the inlet and outlet are defined as pressure inlet and pressure outlet, respectively. The mesh is delineated with the help of the meshing tool, the delineated mesh unit is triangular, and the mesh at the model junction is more dense and detailed, and the simulation results are obtained by result solving. The mesh type selected for the four mesh models is a tetrahedral mesh, and the mesh size is set to the default of 0.38883 m.

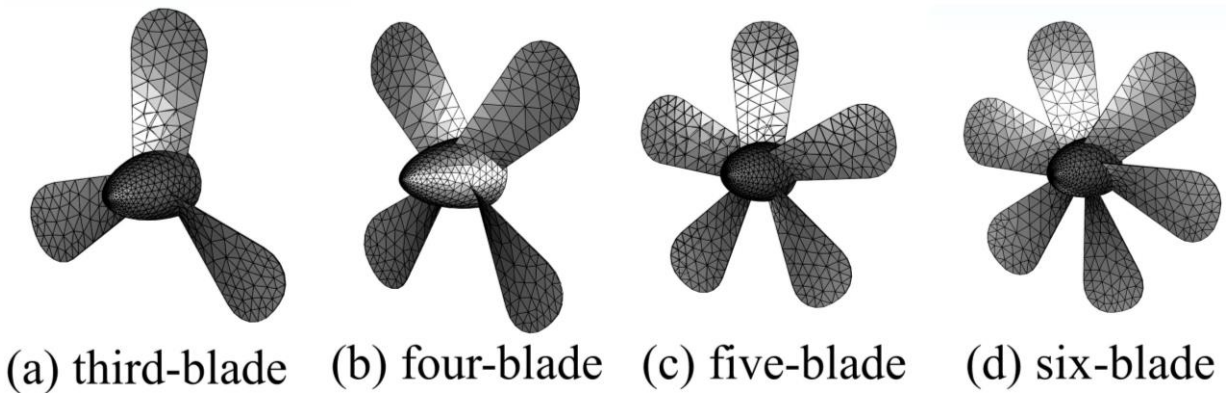

Figure 3: Propeller grid distribution with four: (a) third blade, (b) four-blade, (c) five-blade, (d) six-blade

In this FEA mesh model, the element mass value is 0.999. The mean value of the aspect ratio is 1.945. The mean value of Jacobian is 1, the value of parallel deviation is 0, and the maximum turning angle is 96.641 degrees. The quality of the FEA mesh can be said to be superior. In the meshing stage, the fluid domain is divided into a finite number of discrete cells. The equations are developed at the nodes of the solution domain, and the boundary conditions are applied to start the iterative computation. The number of grid nodes in the rotated domain of the three-leaf model is 7684, and the number of elements is 37525. The number of grid nodes in the rotated domain of the four-leaf model is 8755, and the number of elements is 41432. The number of grid nodes in the rotated domain of the five-leaf model is 8566, and the number of elements is 41603, and the number of grid nodes in the rotated domain of the six-leaf model is 8740, and the number of elements is 41908.

As the propeller is located in the airflow environment, the flow velocity is large. Many small vortices appear in the flow field, and there are two types of contact between neighboring layers, sliding and mixing. The fluid moves irregularly, generating a partial velocity perpendicular to the axis of the flow tube. The simulations were performed using the K-epsilon realisable model, which is a two-range turbulence model widely used in industrial airflows. A two-square equation model implies the inclusion of two additional transport equations to represent the turbulent properties of the flow, such as convection and diffusion of turbulent energy. The first transport variable is the turbulent kinetic energy K, which, in this case, determines the energy in the turbulence. The second transport variable is the turbulent dissipation ϵ, which is the variable that determines the turbulence scale. The K-epsilon model has been shown to work for free shear layer flows with relatively small pressure gradients. Its expression in transport equations is shown below[13].

$$\frac{\vartheta}{\vartheta_t}(\rho k) + \frac{\vartheta}{\vartheta_{x_j}}(\rho k u_j) = \frac{\vartheta}{\vartheta_{x_j}}\left[\left(u + \frac{u_t}{\sigma_k}\right)\frac{\vartheta_k}{\vartheta_{x_j}}\right] + P_k + P_b - \rho_\epsilon - Y_M + S_k \tag{1}$$

$$\frac{\vartheta}{\vartheta_t}(\rho\epsilon) + \frac{\vartheta}{\vartheta_{x_j}}(\rho\epsilon u_j) = \frac{\vartheta}{\vartheta_{x_j}}\left[\left(u + \frac{u_t}{\sigma_\epsilon}\right)\frac{\vartheta_\epsilon}{\vartheta_{x_j}}\right] + \rho C_1 S_\epsilon - \rho C_2 \frac{\epsilon^2}{k+\sqrt{\nu\epsilon}} + C_{1\epsilon}\frac{\epsilon}{k}C_{3\epsilon}P_b + S_\epsilon \tag{2}$$

$$C_1 = max\left[0.43,\ \frac{\eta}{\eta+5}\right] \tag{3}$$

$$\eta = S\frac{k}{\epsilon} \tag{4}$$

$$S = \sqrt{2S_{ij}S_{ij}} \tag{5}$$

Where P_k represents the generation of turbulence kinetic energy due to the mean velocity gradients, calculated in the same manner as the standard k-epsilon model. P_b is the generation of

turbulence kinetic energy due to buoyancy, calculated in the same way as the standard k-epsilon model.

Modelling turbulent viscosity:

$$\mu_t = \rho C_\mu \frac{k^2}{\epsilon} \tag{6}$$

Where

$$C_\mu = \frac{1}{A_0 + A_s \frac{kU^*}{\epsilon}} \tag{7}$$

$$U^* = \sqrt{S_{ij}S_{ij} + \widetilde{\Omega}_{ij}\widetilde{\Omega}_{ij}}; \tag{8}$$

$$\widetilde{\Omega}_{ij} = \Omega_{ij} - 2\epsilon_{ijk}\omega_k; \tag{9}$$

$$\Omega_{ij} = \overline{\Omega_{ij}} - \epsilon_{ijk}\omega_k; \tag{10}$$

Where $\overline{\Omega_{ij}}$ is the mean rate-of-rotation tensor viewed in a rotating reference frame with the angular velocity ω_k. The model constants $A_0$and A_s are given by:

$$A_0 = 4.04 \tag{11}$$

$$A_0 = \sqrt{6}cos\phi \tag{12}$$

$$\phi = \frac{1}{3}cos^{-1}\left(\sqrt{6}W\right) \tag{13}$$

$$W = \frac{S_{ij}S_{jk}S_{ki}}{\widetilde{S}^3} \tag{14}$$

$$\tilde{S} = \sqrt{S_{ij}S_{ij}}, \tag{15}$$

$$S_{ij} = \frac{1}{2}\left(\frac{\vartheta u_j}{\vartheta x_i} + \frac{\vartheta u_i}{\vartheta x_j}\right) \tag{16}$$

Where constant values:

$$C_{1\epsilon} = 1.44 \tag{17}$$

$$C_2 = 1.9 \tag{18}$$

$$\sigma_k = 1.0 \tag{19}$$

$$\sigma_\epsilon = 1.2 \tag{20}$$

4. Aerodynamics modelling of multi-blade type

A cylindrical computational domain with a height of 0.335m and a base diameter of 1.05m is selected for numerical simulation of the process of inflow and outflow of the airflow fluid in a wind tunnel with a height of 6.335m and a base diameter of 3.05m for three-, four-, five-, and six-bladed propellers. Figure 4 presents the modelling of the study on computational domains and fluid orientation. The inlet and outlet boundary conditions for the four-bladed type under quasi-static loading are normal pressure inlet and pressure outlet, and the wall conditions are set to the Z-axis. The blue arrow in Figure 4 indicates the wind tunnel fluid inlet, and the red arrow indicates the outlet. It mainly sets the boundary conditions related to entrance and exit, as well as far-field and wall. The pressure far-field boundary is mainly suitable for simulating compressible flow when using far-field

boundary conditions at the upper, lower, left and right boundaries. The reflection of excitation and expansion waves on the boundary is greatly reduced, and the flow image is the closest to reality. In addition, the entrance and exit of this paper and the far-field are using the pressure boundary[14].

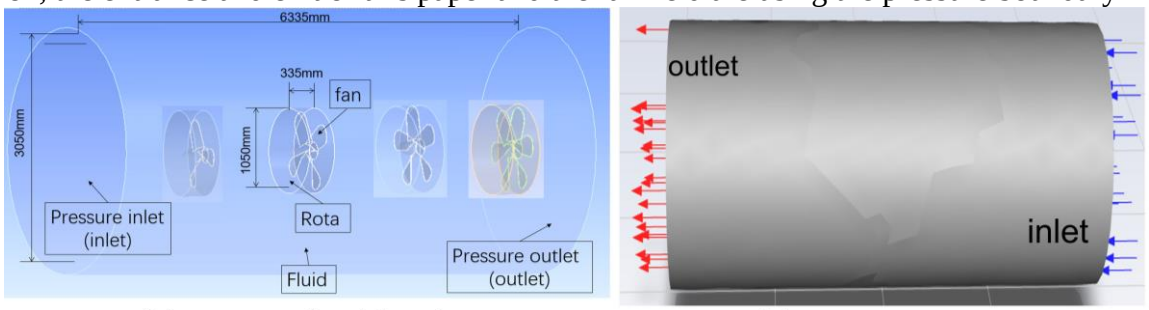

(a) computational domains (b) fluid orientation

Figure 4: Finite element modelling of this study: (a) computational domains; (b) fluid orientation

5. Results and discussion

When the gas flow rate in the wind tunnel is 250 radians/sec, and the contour is 110, the velocity streamlines of the four simulated geometries are derived and analysed. The velocity streamlines of the four different structural propeller models are shown in Figure 5, and the velocity contour is shown in Figure 6. Figure 6 (a) represents the velocity contour of the three-blade propeller, and Figure 6 (b) represents the velocity contour of the four-blade propeller. Figure 6 (c) represents the velocity contour of the five-blade propeller, and Figure 6 (d) represents the velocity contour of the six-blade propeller.

From the velocity streamlines in Figure. 5, it can be seen that propeller models with different numbers of blades affect the direction of fluid flow on the propeller surface under the same flow conditions. Four- and six-blade propellers produce more concentrated fluids, creating the most concentrated and homogeneous fluids of the four geometries. The five-blade propeller then produces the densest fluid. However, a small amount of fluid failed to contact the propeller surface. Of the four structures, the three-blade propeller has the least ability to concentrate the flow: nearly one-third of the flow fails to contact the propeller surface, and the three-blade propeller has the least concentrated flow of the four structures. The three-bladed propeller was the weakest of the four configurations, with nearly one-third of the airflow failing to contact the propeller surface.

From the velocity contour plots in Figure. 6, it can be seen that the maximum fluid velocities on the surface of the propellers with different numbers of blades do not differ much, and the maximum flow velocities of the four propellers are between 136.2 m/s and 149.3 m/s. It can be proved that the velocity contours of the three-bladed and five-bladed propellers in Fig. 5 do not touch the surface of the propellers completely, not because of the fluid velocity in the wind tunnel but because of the insufficient aerodynamic strength of the propellers themselves. The fluid velocities at various points on the specific surface of the propeller can be visualised more by means of the velocity in the stn frame plot, as shown in Figure 7.

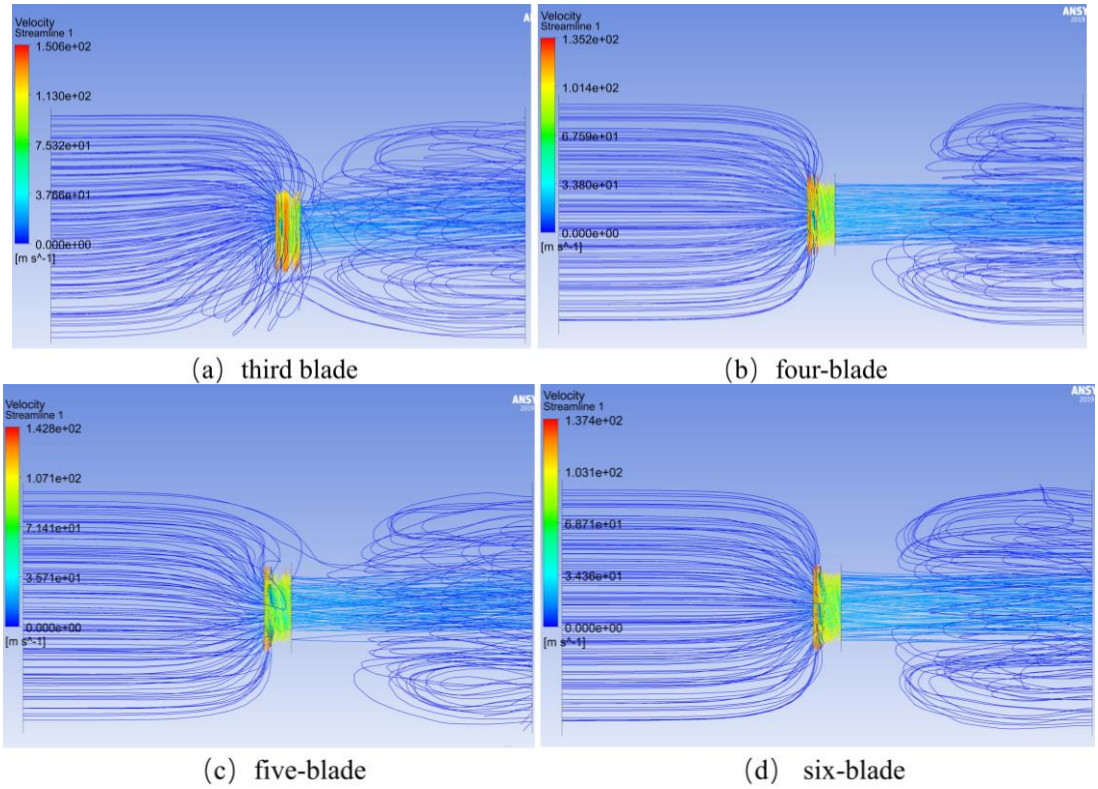

Figure 5: Results of propeller model velocity streamline: (a) three-blade (b) four-blade (c) five-blade (d) six-blade

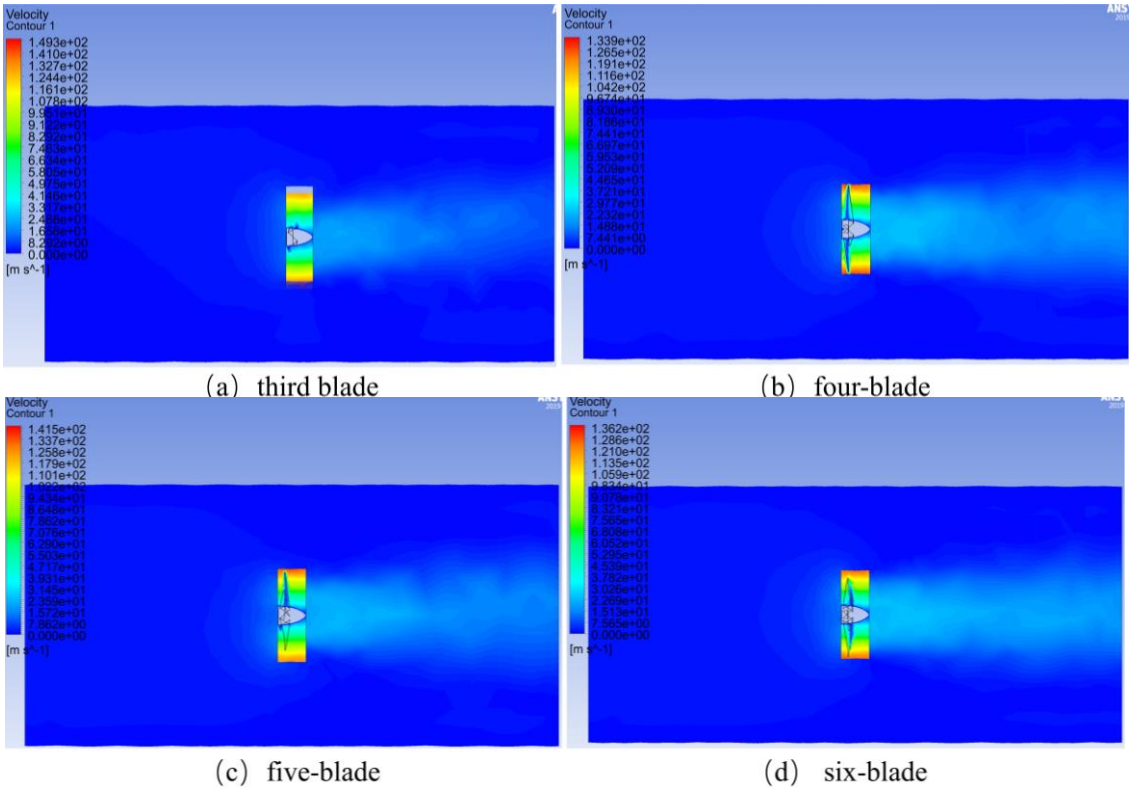

Figure 6: Velocity contour of each blade type propeller surface: (a) three-blade (b) four-blade (c) five-blade (d) six-blade

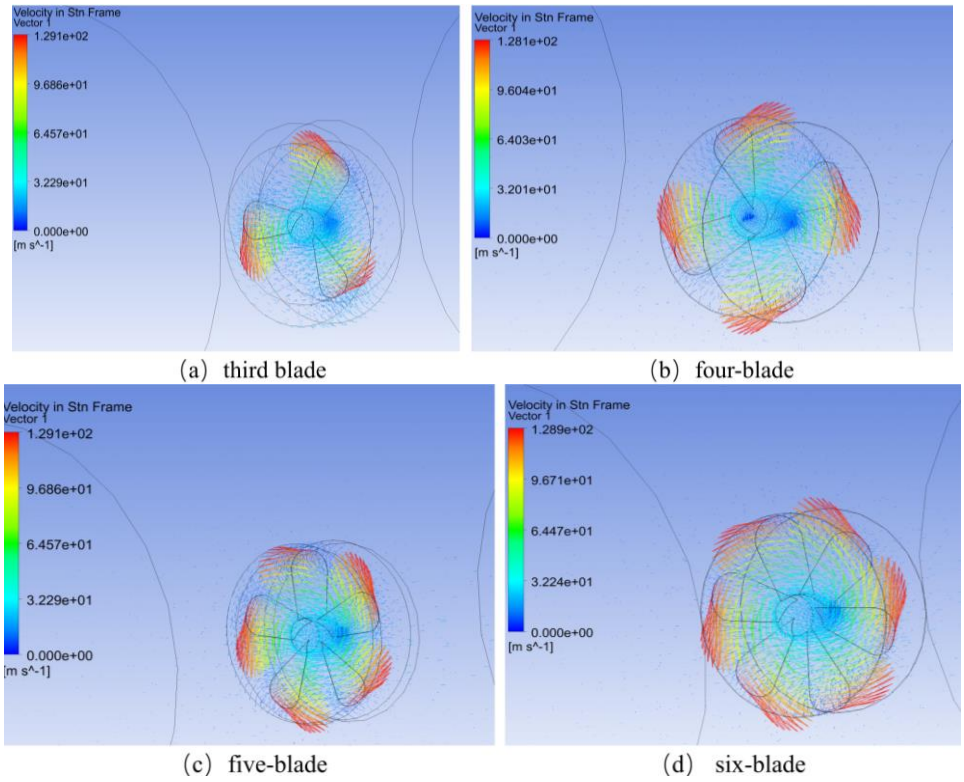

Figure 7: Results of propeller model velocity in stn frame: (a) three-blade (b) four-blade (c) five-blade (d) six-blade

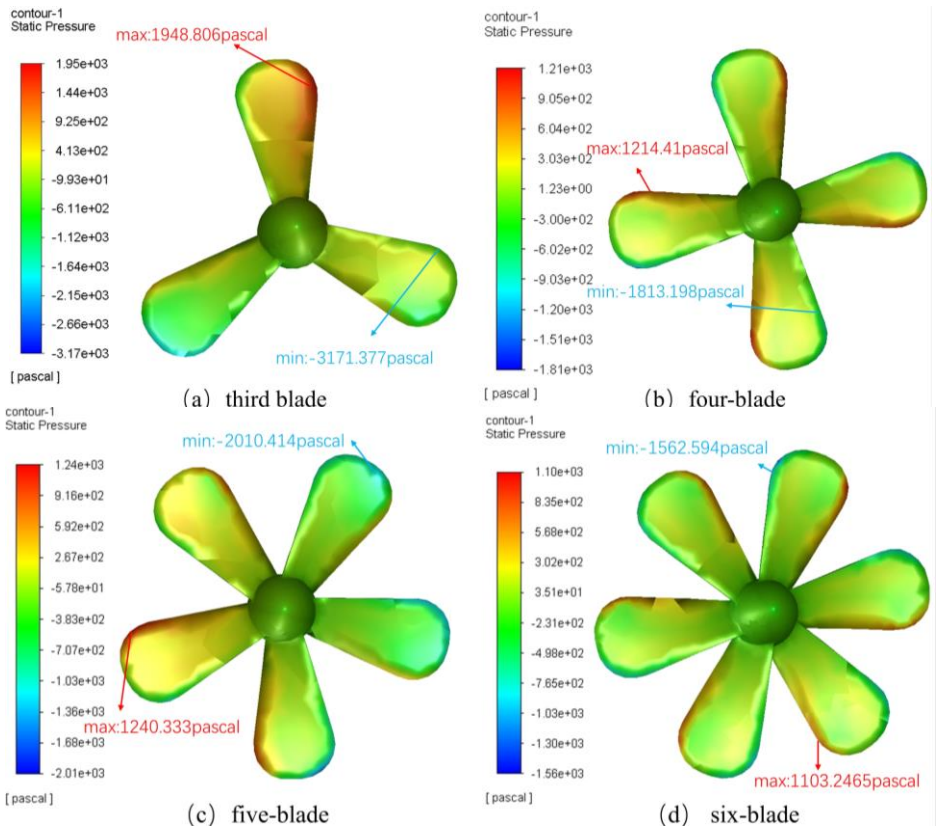

Figure 8: Static pressure contour of each blade type propeller surface : (a) three-blade (b) four-blade (c) five-blade (d) six-blade

The results of the blade static pressure analysis for the four-blade configurations at an airflow rate of 250 radians/sec are shown in Figure. 8. It can be seen that depending on the geometry of the propeller blades, the maximum static stresses on the propeller surface are, in descending order, for the three-bladed propeller (1948.806 Pascal), the five-bladed propeller (1240.333 Pascal), the four-bladed propeller (1214.41 Pascal), and the six-bladed propeller (1103.2465 Pascal). The static stress on the surface of the three-bladed propeller is considerable, and the maximum static stress on its surface is almost one times the maximum static stress on the surface of the six-bladed propeller. It is susceptible to variability and requires the use of higher hardness materials in order to minimise the wear and tear brought about by the stress. In comparison, the other three models of propellers can be selected from lighter and more favourable materials. Pressure contours and pressure vectors for the four paddle types are shown in Figure 9.

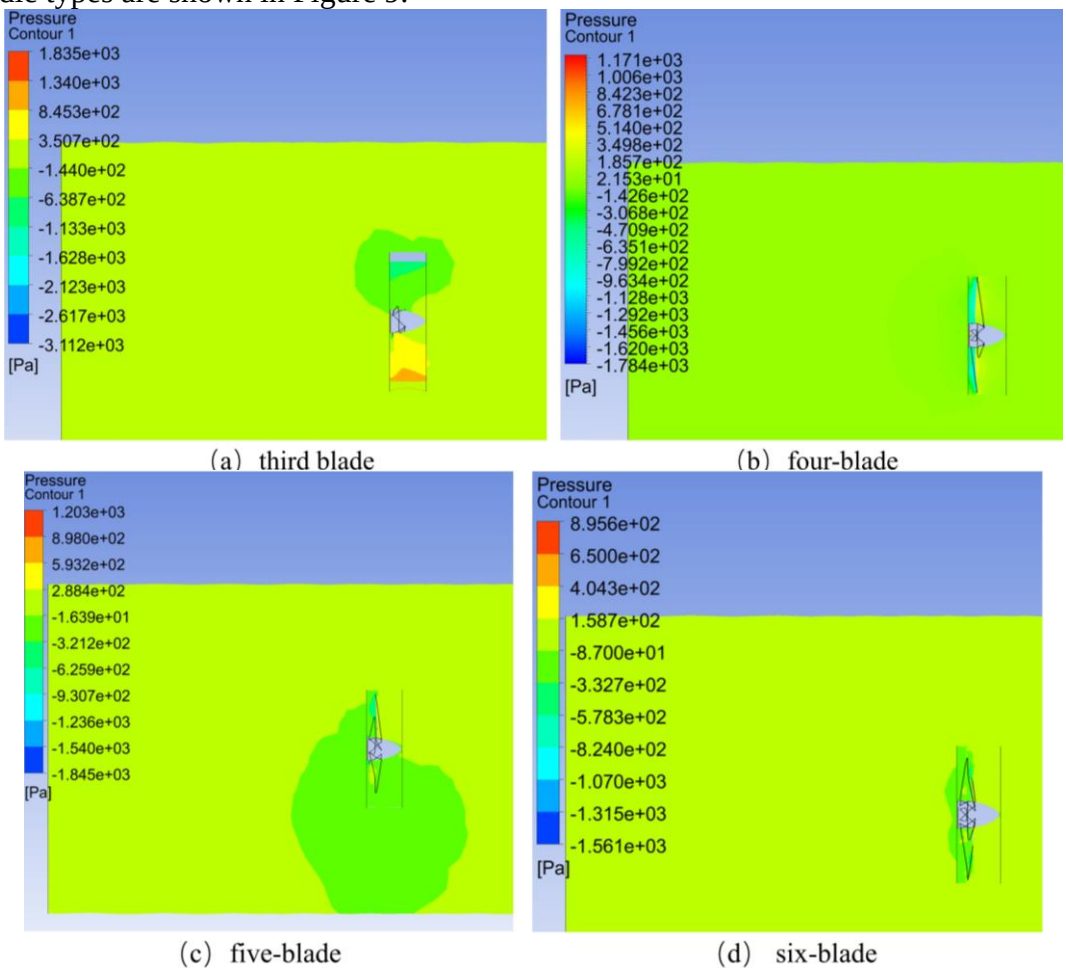

Figure 9: Pressure contour of each blade type propeller surface: (a) three-blade (b) four-blade (c) five-blade (d) six-blade

6. Conclusion

The aerodynamic characteristics of propellers are investigated in a constant flow velocity airflow wind tunnel using the CFD method. Three-blade, four-blade, five-blade and six-blade propellers based on the same material were selected and hydrodynamically simulated with the help of fluent simulation software for these four propellers. It is obtained that under the same flow conditions, the four-blade propeller and the six-blade propeller will make the fluid more concentrated. The four-, five-, and six-blade propellers can be selected from lighter materials than the three-blade propellers,

which means that the four-bladed is better under the premise of smaller propeller volume. The maximum pressure on the surface of the propeller is in the order of three-blade propeller, five-blade propeller, four-blade propeller and six-blade propeller. It is concluded that the aerodynamic performance of the four-bladed propeller is optimal under the condition of 250 rad/sec fluid velocity. Designing an optimized propeller blade structure is an effective way to improve the efficiency of the vehicle. The computational results help to provide insight into the physical characteristics of the airflow around the propeller blades and the resulting performance metrics.

References

[1] Wang Yanbing. Analysis and Optimization of Propeller Aerodynamic Characteristics for General Electric Airplanes[D]. Shenyang University of Aeronautics and Astronautics. 2021.

[2] LIU Peiqing, GENG Xin, HU Tianxiang, et al. Research progress on aerodynamic, noise and optimization design of modern aviation propellers[J].Journal of Aerodynamics2023,41(10):62-78+61.

[3] Gan Wenbiao, Zhuang Junjie, Zuo Zhenjie, et al. Advances in propeller flow control for low dynamic vehicles in near space[J/OL]. Journal of Aeronautics. 1-19[2024-07-12].http://kns.cnki.net/kcms/detail/ 11.1929.V. 20240523. 1256. 017.html.

[4] Lu Yanjun, Zhang Xiaodong, Ji Pengfei, Wang Zhenwei. Experimental System for Testing Propeller Lift Characteristics of Multi-rotor Vehicles[J]. Laboratory Research and Discovery,2017,36(01):69-72+79.

[5] Liu Y , Yuan Q , Xu Z ,et al.Bionic Volute Tongue Optimization Design of Multi-blade Centrifugal Fan Inspired by the Wave Leading-edge of Humpback Whale Flippers[J].Journal of Bionic Engineering, 2023, 20(5):2209-2227. DOI:10.1007/s42235-023-00354-w.

[6] Zhiyuan W U , Zhao L , Yan H ,et al.Multi-blade rubbing characteristics of the shaft-disk-blade-casing system with large rotation[J].Applied Mathematics and Mechanics(English Edition), 2024, 45(1):111-136.DOI:10.1007/s10483-024-3071-5.

[7] LIU Peiqing, GENG Xin, HU Tianxiang, et al. Research progress on aerodynamic, noise and optimization design of modern aviation propellers[J].Journal of Aerodynamics2023,41(10):62-78+61.

[8] Zhang X , Zheng M .Numerical Simulation of Fluid-Structure Coupling for a Multi-Blade Vertical-Axis Wind Turbine[J]. Applied Sciences, 2023.DOI:10.3390/app13158612.

[9] Kostić I .Numerical evaluation of the aerodynamic influence of the helicopter composite blade trailing edge tabs[J].Archive of Applied Mechanics,2007,77(12):893-909.

[10] Xu Zhengyu, Tang Sijia, He Miao, etc. Propeller Aerodynamic Parameters and Integrated Aircraft Design Techniques[J]. Journal of Aerodynamics. 2023,41(10):88-99.

[11] Wu Jiayu, Yang Jinshui, Chen Dingding et al. Research progress on manufacturing process of aerospace composite propeller blade[J].Journal of Aerospace Materials.2024,44(02):104-116.

[12] Khaleel H H .Stress Analysis of Gas Turbine Propeller Using Finite Elements Method[J].Mathematical Modelling of Engineering Problems,2023,10(1):236-241.

[13] CFD Online. Realisable k-epsilon model [EB/OL] .https://www.cfd-online.com/Wiki/Realisable_k-epsilon_model. 2024, 6,16.

[14] CAE Simulation Online. What is FLUENT's "pressure far-field boundary"?[EB/OL]http://www.1cae.com/a/ansys-fluent/53/fluent-9108.htm.2024,6,16.